# Photophysical Study in Blends of Poly(alkyl methacrylate-*co*-styrene)/Polystyrene

**Marcelo L. de Andrade and Teresa D. Z. Atvars***

*Instituto de Química, Universidade Estadual de Campinas, Campinas, São Paulo, Brazil*

*Received April 15, 2004; Revised Manuscript Received August 4, 2004*

ABSTRACT: The morphology of blends of poly(alkyl methacrylate-*co*-styrene)/polystyrene [XMAS/PS; X = M (methyl), E (ethyl)] was studied at the microscopic level (micrometric scale) by differential scanning calorimetry (DSC), dynamic-mechanical analysis (DMA), and epifluorescence microscopy (EFM) and at the nanoscopic scale by steady-state and time-resolved fluorescence emission spectroscopy (FES). Time-resolved energy transfer analysis was used to probe the interpenetration of molecular chains. The copolymers MMAS and EMAS (approximate content in mol %: 78% of methacrylate units; 22% of styrene units) covalently labeled with 9-vinylanthracene units (≤0.1%), as fluorescent comonomer (fluorophore), were synthesized by emulsion polymerization and were characterized by FTIR, $^1$H NMR, $^{13}$C NMR, TGA, GPC, DSC, DMA, UV−vis, and FES. Films of copolymer blends were prepared by casting from dilute chloroform solutions with compositions of 5, 20, 50, 80, and 95 wt % of copolymer. Some miscibility was observed for the blends of XMAS/PS containing 5, 20, and 95 wt % of copolymer. Interaction strength in blends increased with the size of aliphatic chain of the ester group in the copolymer. Blends with 50 wt % of copolymer are always immiscible. Two values of glass transition temperatures were observed by DSC and DMTA. MMAS/PS and EMAS/PS blends of copolymer-richer compositions (95 and 80 wt %) show fluorescence lifetimes with broader distributions, suggesting a wider distance distribution of interlumophoric groups.

## Introduction

Blending of two or more thermoplastics may produce new materials with a combination of properties not found in the neat polymers, and it also constitutes a faster and more cost-effective way of achieving the required properties than synthesizing new polymers. Because the polymer properties are critically dependent on the morphology of the material, knowledge of blend morphology can greatly aid the tailoring of polymer blends. The morphology of immiscible polymer blends shows a remarkable diversity, but fundamentally a distinction between blends with discrete phase structure and blends with cocontinuous or bicontinuous phase structure can be made.[1,2]

It is well-known that most polymer blends are immiscible due to a high degree of polymerization. Therefore, the entropy term becomes vanishingly small, and the miscibility is increasingly dependent on the nature of the enthalpic term contribution. As a result, phase behavior of polymer blends is strongly affected by intermolecular association. To enhance the formation of one phase system in polymer blends, it is necessary to ensure that favorable specific intermolecular interactions exist between two base components of the blend, such as $\pi$-electron interaction.[2,3]

Polystyrene (PS) and poly(methyl methacrylate) (PMMA) are widely used individually or as components of a blend with other high-performance polymers. However, their application to blends is often limited because of their immiscibility with other polymers.[4−6] Copolymerization with other polymers based on a binary interaction model[7] is often used to improve the miscibility with other high-performance polymers, and thus various methacrylates are often copolymerized with PS.[8]

There are several criteria to establish miscibility in polymer blends. For a better understanding of the degree of mixing, a good characterization of the spatial distribution of the two components on very small spatial scale is necessary. Some of the most widely employed techniques are differential scanning calorimetry (DSC) and dynamic-mechanical thermal analysis (DMTA), and the most important parameter is the glass transition temperature ($T_g$). A single $T_g$ value is the necessary condition for a miscible blend system, and this temperature is compared to the $T_g$ of the neat components. However, this parameter requires higher miscibility; otherwise, the technique has no sensitivity and is only an indirect measurement of spatial distribution. Fluorescence nonradiative energy transfer (NRET) is a technique able to discriminate miscibility at the nanometric scale[9−13] and is sensitive to distances on the order of 2 nm. It has also been generally observed that the fluorescence lifetimes of heterogeneous blends are usually nonexponential because there are multiple distances separating the energy donor and energy acceptor pairs.[14] Therefore, the distribution of fluorescence lifetimes seems to be the best way for analyzing the experimental data without any arbitrary assumption of two or three exponential terms to fit the experimental curve profile.[6] Nevertheless, higher spatial resolution can be achieved using atomic force,[9a,15] electron scanning,[16] or transmission microscopies.[17]

Direct analysis of polymer blend morphology can be performed by several types of microscopies. Nevertheless, electron microscopy can undergo same problems when phase separation is artificially introduced in blends by staining or by heating the sample during the focalization of the electron beam[18] or when there is a lack of natural contrast between the components of

* Corresponding author: e-mail tatvars@iqm.unicamp.br; Fax 55-19-37883023; phone 55-19-37883078.

10.1021/ma049265e CCC: $27.50 
Published on Web 11/04/2004

**Table 1. Some Physical Properties of Polystyrene (PS) and Its Methacrylate MMAS and EMAS Copolymers**

| polymer | $x$ (mol %)[a] | $y$ (mol %)[a] | $z$ (mol %)[a] | $\bar{M}_n$ (kg/mol)[b] | $\bar{M}_w/\bar{M}_n$[b] | $T_g$ (°C) DSC | $T_g$ (°C) DMTA |
|---|---|---|---|---|---|---|---|
| MMAS | 78.5 | 21.4 | < 0.1 | 77.4 | 2.3 | 85 | 103 |
| EMAS | 78.5 | 21.5 | < 0.1 | 95.6 | 2.4 | 61 | 73 |
| PS | | 100 | | 64.6 | 2.6 | 91 | 95 |

[a] From UV−vis. [b] From GPC.

the mixture that contributes to experimental difficulties.[19] Acrylates are particularly sensitive to an electron beam and can be degradated. Optical microscopies are simpler techniques although the spatial resolution is poorer. In the conventional form, the lack of utility occurs when the refractive indices of both components are very similar.[19] One particular type of optical microscopy is epifluorescence (EFM), which combines the facility of the optical microscopy with the ability to identify the chemical nature of polymer domains.[18,20,21] More recently, we employed epifluorescence microscopy, microspectrofluorimetry,[22] thermal analysis methodologies, and distribution analysis of the emission decays for studying the miscibility of poly(*n*-butyl methacrylate-*co*-styrene) (nBMAS) with polystyrene (PS) blends.[23]

In the present work, NRET from binary blends of PS, which contain phenyl groups as possible energy donors, and poly(alkyl methacrylate-*co*-styrene) (XMAS) [X = M (methyl), E (ethyl)] labeled with anthryl units, as energy acceptor groups, was studied. Epifluorescence microscopy (EFM), steady-state microspectrofluorescence, and time-resolved spectroscopic techniques were used. Samples in the form of films were prepared by casting dilute solutions containing PS with several relative amounts of copolymers by mass (from 5% to 95%). Lifetime distribution analysis was used to fit the experimental fluorescence decay curves. Intermolecular correlations between the donors and traps were used to analyze the interchain structures in miscible blends and in blends with phase separation. For complementary analysis of the phase separation processes, glass transition temperatures were determined by DSC and DMTA.

## Experimental Section

**Materials.** Monomers (methyl methacrylate, MMA, Aldrich Chemical Co.; ethyl methacrylate, EMA, Aldrich Chemical Co.; and styrene, STY, Aldrich Chemical Co.) were washed with 5% sodium hydroxide, followed by distilled water. Afterward, they were first dried over anhydrous sodium sulfate, then purified by vacuum distillation, and stored in a refrigerator. The fluorescent monomer 9-vinylanthracene (9-VAn, 97%, Aldrich Chemical Co.), potassium persulfate (KPS, 99%, Aldrich Chemical Co.), sodium dodecyl sulfate (SDS, 98%, Merck), sodium bicarbonate (99%, Synth), and dodecyl mercaptan (DM, 99.5%, Aldrich) were used as supplied. Chloroform (Merck) and methanol (Merck) were of analytical grade. Atactic polystyrene (PS, $\bar{M}_n$ = 64 kg/mol) was purchased from EDN (Brazil) and was used as received.

**Synthesis and Characterization of the Copolymers.** The conventional emulsion copolymerization of the monomers XMA [X = M (methyl) or E (ethyl)], STY, and 9-VAn as well the separation of the products were carried according to the protocol already described.[23] Characterization of the copolymers was performed by FT-IR and by high-resolution $^1$H and $^{13}$C NMR under conditions already described.[23]

The molar contents of the monomeric units of methacrylate groups, styrene, and anthryl groups in the copolymers were determined using a Hewlett-Packard-8452A UV−vis spectrophotometer, using molar absorption coefficients of $\epsilon_{207}$ = 69 L mol$^{-1}$ cm$^{-1}$ (ethyl acetate), $\epsilon_{262}$ = 260 L mol$^{-1}$ cm$^{-1}$ (toluene), and $\epsilon_{386}$ = 9700 L mol$^{-1}$ cm$^{-1}$ (9-methylanthracene).

Molecular weight and molecular weight distributions of the copolymer and polystyrene (Table 1) were evaluated by gel permeation chromatography (GPC), using a linear $\mu$Styragel column (American Polymer Standards Co.) at 40 °C coupled to a refractive index detector (Waters 410), with THF as the eluent. Monodisperse polystyrene standards were used as the calibration standards.

**Preparation and Analysis of Blends.** Films (approximate thickness of 0.3 mm) of XMAS/PS blends containing several compositions of copolymer (5/95, 20/80, 50/50, 80/20, and 95/5 wt %) were prepared by casting 10% chloroform solutions on silanized Petri dishes (to avoid adhesion). The solvent was slowly evaporated (2 days at room temperature), and then the films were dried for a day in an oven at 50 °C under dynamic vacuum. They were annealed at 100 °C under dynamic vacuum in an oven for 12 h to minimize thermal stress and erase prior thermal histories.

The glass transitions of these films were determined by differential scanning calorimetry (DSC) and dynamic-mechanical thermal analysis (DMTA). DSC measurements were carried out in a model v2.2A 90 DSC from DuPont, calibrated with indium as standard, following the protocol already described.[23] Dynamic mechanical spectra were obtained with a Thermal Analyst 2100-DMA983 from TA Instruments, operating in sinusoidal oscillation at 1 Hz, using a 3 °C min$^{-1}$ heating rate. Specimens with average dimensions of 4.5 × 0.3 × 7.0 mm were previously annealed at 100 °C for 10 h.

**Surface Morphology and Photophysics.** Epifluorescence microscopy (EFM) was performed using an inverted Leica DM IRB microscope employing a mercury arc lamp HBO (HBO-100 W) for UV−vis excitation in the wavelength range of 330−380 nm selected by optical filters. The emission image was selected from the excitation beam by a dichroic mirror ($\lambda_{exc}$ > 410 nm). Objective magnifications of 25×, 50×, and 100× were used, and the images were taken with a Sansung SDC-311 digital camera and processed by Linksys v. 2.38 software. Images can be interpreted as blue regions due to the fluorescence from anthryl-labeled copolymers XMAS and the dark (nonfluorescent regions) from the PS domains.

Steady-state fluorescence microspectroscopy (FMS) was performed using an ISS-PC1 spectrofluorimeter coupled to the epifluorescence microscopy. To get areas as small as few micrometers, the microscope objective was selected for a magnification of 630×. Samples were only illuminated by the mercury arc lamp HBO-100 W, with the excitation wavelength selected in the region 340−380 nm to provide, preferentially, excitation of 9-anthryl moieties. Images were collected from the surface and from the bulk at several depths by changing the microscope focus. Fluorescence spectra corresponding to each one of the images were recorded in the region 410−550 nm.

Steady-state fluorescence spectra were also performed for the whole film in the same spectrofluorimeter using back-face illumination. The samples were excited at 262 nm, and the fluorescence emission was collected in the range 270−500 nm. Excitation spectra were collected in the range 340−410 nm, using $\lambda_{em}$ = 420 nm.

Fluorescence lifetimes were obtained by time-correlated single photon counting (TCSPC) in a FL 900 spectrofluorimeter (Edinburgh Analytical Instruments, Edinburgh, U.K.). Excitation was carried out by a pulsed hydrogen flash-lamp controlled by a Thyratron tube operating with a repetition frequency rate of 40 kHz. The sample is maintained in a sealed

quartz cuvette under vacuum. Measurements were performed with $\lambda_{exc} = 262$ nm, collecting the emission signal in two wavelengths: at $\lambda_{em} = 340$ nm (for the decay from the excimeric phenyl groups) and at $\lambda_{em} = 420$ nm (for the decay from the anthryl groups). For a lifetime analysis based on the single-photon-counting technique, the model response function $G(t)$ is the theoretical impulse decay function $I(t)$ convoluted with instrument response function $R(t)$, as previously described.[23]

## Results and Discussion

**Polymer Characterization.** The copolymers were characterized by FTIR spectroscopy showing several typical vibrational modes: antisymmetric and symmetric stretching vibrations of the $CH_3$ groups (2993 and 2982 $cm^{-1}$) overlapped with the antisymmetric and symmetric stretching vibrations of the $CH_2$ groups (2948 and 2937 $cm^{-1}$); C=O stretching vibrations (1772−1670 $cm^{-1}$); in-plane bending vibrations of $CH_3$ groups (1453 $cm^{-1}$); in-plane bending vibrations of $CH_2$ groups (1484−1477 $cm^{-1}$); rocking vibrations of $CH_2$ (755 $cm^{-1}$); skeletal vibrations of the polymer backbone (1147 $cm^{-1}$); −C−O−C− stretching (1074 $cm^{-1}$); and symmetric bending of C−H bonds from $CH_3$ groups (1385 $cm^{-1}$). The FTIR also shows absorption bands characteristic of the phenyl groups belonging to the styrene block: −C−C− stretching vibrations (1601 $cm^{-1}$); out-of-plane C−H angle deformation (701 $cm^{-1}$) and aromatic −C−H stretchings (3024 $cm^{-1}$).[24]

The proton NMR spectra of MMAS and EMAS copolymers show chemical shifts from phenyl protons in the region of 6.92−7.27 ppm (MMAS and EMAS), the methyleneoxy protons (−$OCH_2$−) in the region of 3.82−4.18 ppm (EMAS), and the methoxy protons (−$OCH_3$) from MMAS copolymer in the region of 3.40−3.68 ppm. The chemical shifts from the methyne protons of the styrene units in the copolymers are found in the region of 2.78−3.03 ppm (MMAS) and 3.02−3.42 ppm (EMAS), and the chemical shifts from the methylene groups (−$CH_2$−) in these copolymers are observed in the region of 1.21−2.15 ppm (MMAS) and 1.08−2.09 ppm (EMAS). The resonance peaks from methyl groups in these copolymers appear in the region of 0.47−1.02 ppm (MMAS and EMAS).

The $^{13}C$ NMR spectra of MMAS and EMAS copolymers show resonance peaks from carbonyl groups: (C=O) at 176.09−177.64 ppm (MMAS) and 175.74−177.75 ppm (EMAS); phenyl carbons from styrene units (−C=) at 125.94−144.77 ppm (MMAS) and 125.86−146.43 ppm (EMAS); methoxy groups (−$OCH_3$) at 54.21 ppm (MMAS) and methyleneoxy groups (−$OCH_2$−) at 59.95−60.54 ppm (EMAS); methyne groups of styryl units ($\phi$-$C_\alpha$−H) at 50.61−51.71 ppm (MMAS) and 51.21−54.15 ppm (EMAS); methylene groups (−$CH_2$−) from the polymer backbone at 44.39−45.42 ppm (MMAS) and 44.57−45.58 ppm (EMAS); methyl groups (−$CH_3$) at 16.31−18.67 ppm (MMAS) and 13.48−18.48 ppm (EMAS). The solvent peak ($CDCl_3$) appears in the region of 76.49−77.92 ppm.

Molar percent contents of each monomer unit in the copolymers ($x$, $y$, and $z$ in Figure 1 and Table 1) were determined by UV−vis absorption spectra and taking the absorbances at 207, 262, and 386 nm, corresponding to absorption of the ester group ($A_{207}$), styryl ($A_{262}$), and 9-anthryl ($A_{386}$) units, respectively, and then using relationships deduced from substitution of the Beer−Lambert's law ($c = A/\epsilon l$) (where $\epsilon$ and $c$ are the molar absorption coefficients and concentration of the involved

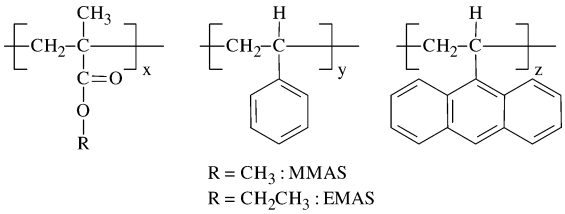


**Figure 1.** Chemical structure of component monomers in the random copolymers: MMAS and EMAS. The molar contents $x$, $y$, and $z$ are listed in Table 1.

species) into $x = c_x/(c_x + c_y + c_z)$, $y = c_y/(c_x + c_y + c_z)$, $z = c_z/(c_x + c_y + c_z)$, resulting in

$$x = \frac{140.6A_{207}}{140.6A_{207} + 37.3A_{262} + A_{386}} \quad (1)$$

$$y = \frac{37.3A_{262}}{140.6A_{207} + 37.3A_{262} + A_{386}} \quad (2)$$

$$z = \frac{A_{386}}{140.6A_{207} + 37.3A_{262} + A_{386}} \quad (3)$$

In Table 1 are listed the number-average molecular weights ($\bar{M}_n$) of MMAS, EMAS, and PS obtained by gel permeation chromatography (GPC), all arising from unimodal distributions with relatively low polydispersities ($\bar{M}_w/\bar{M}_n$).

The reactivity ratios ($r_1$ and $r_2$) for the radical copolymerization between methyl methacrylate ($r_1 = 0.49$)/styrene ($r_2 = 0.53$) and ethyl methacrylate ($r_1 = 0.29$)/styrene ($r_2 = 0.65$) pairs are lower than unity, and hence it is expected a random copolymer with alternation of both monomeric mers will be formed. Therefore, blocks cannot be thought of as large. This argument will be used later to explain the absence of excimer phenyl groups emission from the XMAS copolymers.

Glass transition temperatures ($T_g$) were determined for both copolymers and of PS homopolymer (trace 7 in Figure 2a,b; Table 1). According to DSC traces, both copolymers are amorphous materials exhibiting glass transition temperatures below that for the PS homopolymer (91 °C): 85 and 61 °C for MMAS (trace 1, Figure 2a) and EMAS (trace 1, Figure 2b). These $T_g$ values are close to the corresponding polymethacrylate homopolymers with molecular weight above the critical value.[25]

Different from the DSC data, the $T_g$ values from the DMTA measurements (Figure 3a,b) are about 10 °C higher, as shown in Table 1. Such differences arise presumably due the kinetic features of the glass transition process, which is described as a function of the time or frequency (for DMTA) or heat ratio (for DSC), rather than to having a single temperature value.[26] Besides the glass transition temperatures of the polymers, the DMTA traces show also a shoulder at lower temperatures assigned to the $\beta$-secondary relaxation from smaller segments in the main chain.[27]

**Photophysical Behavior of the Polymers.** Figure 4 shows the steady-state fluorescence spectra of the PS homopolymer and of the MMAS and EMAS copolymers. The broad band of the PS spectrum centered at 310 nm can be decomposed into two components: a higher energy (approximately 280 nm) and a red edge (approximately 320 nm) that can be respectively attributed to the isolated phenyl groups and to the excimeric

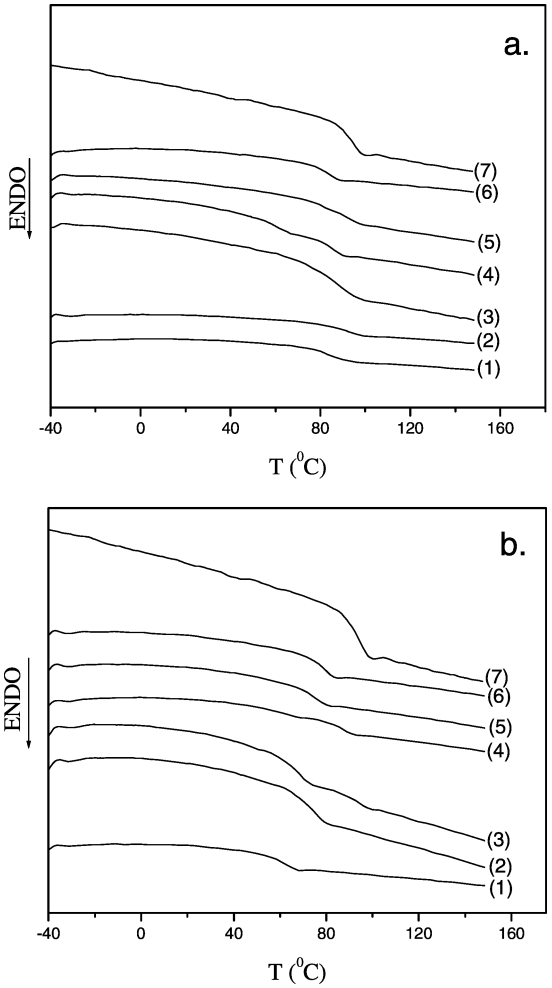


**Figure 2.** DSC traces (second run) for homopolymer PS (trace 7), copolymer (trace 1), and blends of (a) MMAS/PS and (b) EMAS/PS with (2) 5, (3) 20, (4) 50, (5) 80, and (6) 95 wt % PS.

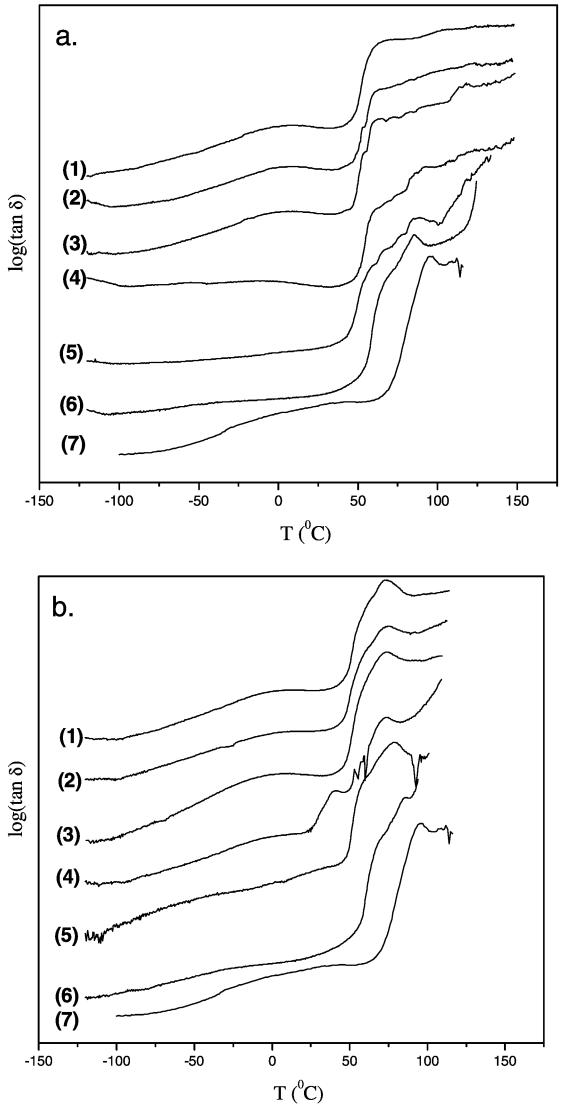


**Figure 3.** Temperature dependence of the loss tangent (tan $\delta$) (1 Hz; 3 °C/min) for homopolymer PS (trace 7), copolymer (trace 1), and blends of (a) MMAS/PS and (b) EMAS/PS blends with (2) 5, (3) 20, (4) 50, (5) 80, and (6) 95 wt % PS.

species. Excimers in PS are formed between two coplanar phenyl rings arranged in a suitable geometry along the polymer coil during the lifetime of the electronic excited state.[28] Either intramolecular or intermolecular excimers have been observed in the solid state.

Regardless the copolymer, MMAS or EMAS, the fluorescence spectra of the copolymers are composed of two bands, when excited at $\lambda_{exc} = 262$ nm (Figure 4): a higher energy emission centered at 289 nm due to the phenyl groups from styrene blocks and a lower energy band centered at 420 nm attributed to the 9-anthryl groups. The emission band of the 9-anthryl groups is broader compared to the 9-anthryl derivatives in the molecular form[29] although it is similar to other anthryl-based polymers.[23,30] This broadening arises from the presence of several chain conformations that produce different microenvironments for the lumophore that cannot relax to the more stable Franck−Condon state during the excited-state lifetime of the copolymers, imposing restrictions on the molecular orientation during the lifetime of the electronic excited states.

The complete absence of excimeric emission of the phenyl groups in the copolymer is noteworthy, even though the phenyl groups are simultaneously excited by irradiation with 262 nm. This result gives additional information on the distribution of the styrene, methacrylate, and vinylanthryl blocks in the copolymer chain. As described earlier, these are random copolymers. Because of the random organization and the similarity among the reactivity parameters, these blocks are shorter than those necessary to produce excimeric emission of the phenyl groups.

Unlike emission spectra, the excitation spectra of the copolymers ($\lambda_{em} = 420$ nm) possess sharper vibronic structures (350−400 nm) usually observed for anthryl derivatives.[31] The copolymer excitation spectra are partially overlapped with the PS emission spectrum (see dark area in Figure 4). This spectral overlap is a necessary condition for the occurrence of the electron energy transfer process induced by dipole−dipole interaction, as described by the Förster mechanism, between donors (excimer phenyl groups) and acceptors (9-anthryl moieties).[28b] It is also noteworthy that phenyl group emission from the copolymers (centered at 280 nm) does not overlap with the anthryl excitation spectra (350−400 nm), and consequently, only lower efficiency energy transfer processes take place between the copolymer chains. We will go back to this point when discussing energy transfer processes in PS/copolymer

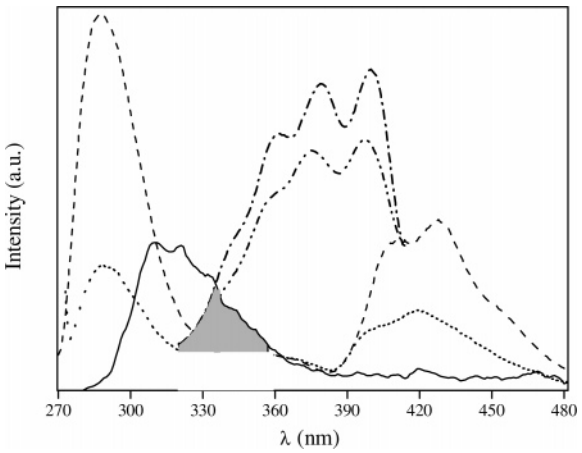


**Figure 4.** Excitation ($\lambda_{em}$ = 420 nm) and steady-state fluorescence ($\lambda_{exc}$ = 262 nm) of neat polymer films: (—) PS emission; EMAS (- · -) excitation and (- - -) emission; MMAS (- ·· -) excitation and (· · ·) emission. The filled area corresponds to spectral overlapping between the PS emission (donor) spectrum and the copolymer (MMAS or EMAS) excitation spectrum (acceptor).

blends since the spectral overlap between the excimeric species in PS and the anthryl moieties in the copolymers are rather stronger.

Figure 5 shows the fluorescence decays for PS and the copolymers obtained by single photon counting measurements. The decay curve of PS monitored at $\lambda_{em}$ = 340 nm, which is characteristic of the excimer phenyl groups (Figure 5a), can be fitted to a bimodal lifetime distribution with two average lifetime values: $\langle\tau_{ann}\rangle$ = 3.7 ± 1.0 ns and $\langle\tau_{exm}\rangle$ = 21.0 ± 4.7 ns, attributed to the singlet−singlet annihilation and the normal excimer decay, respectively.[22] Because the nonradiative energy transfer process decreases the fluorescence quantum yield of the donor as well as the lifetime of the excited state, only the slower component ($\tau_{exm}$ = 21.0 ns) will be important when evaluating blend miscibility through the differences in lifetimes in the presence and the absence of energy transfers from the excimer phenyl moieties to the 9-anthryl acceptor moieties.

Figure 5 also shows that the fluorescence decays of the 9-anthryl groups in MMAS and EMAS copolymers collected at $\lambda_{em}$ = 420 nm. Different from the emission of the excimer phenyl groups (absence in these copolymers), the lifetime distributions for 9-anthryl groups are narrower (monomodal), giving a single average fluorescence lifetime: $\langle\tau_{ant}\rangle$ = 10.7 ± 1.4 ns (MMAS) and $\langle\tau_{ant}\rangle$ = 10.6 ± 1.6 ns (EMAS). These are typical values for the fluorescence lifetime of anthryl moieties.[23,29,31]

**Thermal Properties and Morphology of the MMAS/PS and EMAS/PS Blends.** Figure 6a,b shows the EFM micrographs for the MMAS/PS and EMAS/PS blends with 5 wt % of copolymer. They are morphologically similar, resembling quasi-uniform mixtures, with highly diffuse interconnected fluorescent phases (blue regions) produced in the course of the spinodal decomposition.[32] The morphology of a blend of PS with 5 wt % poly(*n*-butyl methacrylae-*co*-styrene-*co*-9-vinylanthracene) (nBMAS/PS) was similar, with interconnected zones of more intense fluorescence.[23] Hence, the three blends (MMAS/PS, EMAS/PS, and nBMAS/PS), at this composition, are considered as a biphasic system where each phase contains both components but different composition according to the optical microscopic resolution and $T_g$ criterion. As will be shown later, the differences among them and the correlation of the size of the ester−aliphatic chain with phase separation will be more evident by using fluorescence spectroscopy techniques.

Although the DSC traces for the blends containing 5 wt % of XMAS (trace 6 in Figure 2a,b) show single $T_g$ values (Table 2), the DMTA data (trace 6 in Figure 3a,b) exhibit two glass transitions each (Table 2), in better agreement with morphologies that reveal interconnected phases. The higher sensitivity of DMTA of microheterogeneous polymer blends has already been discussed.[33]

EFM micrographs of MMAS/PS blends with 20 wt % MMAS are shown in Figure 7a,b. Again a cocontinuous morphology is observed with two interconnected phases, which are maintained after annealing (Figure 7b): one blue fluorescent (copolymer-rich) and one nonfluorescent (pure PS). The biphasic morphology was also observed by two $T_g$ values in DMTA traces (trace 5 in Figure 3a and Table 2): one below the $T_g$ of the copolymer (lower $T_g$), suggesting some specific interaction between PS and copolymer chains within the fluorescent interconnected copolymer-rich phase, and other below the neat PS, also suggesting a miscibility between these two materials. Nevertheless, a single $T_g$ value and broad trace profile are found by DSC (trace 5 in Figure 2a and Table 2).

In addition to the images, we also obtained the fluorescence spectrum using a microspectroscopy system (Figure 7c for MMAS blend) for different parts of the sample and also at different depths from the surface. Each square microzone (50 × 50 $\mu$m) is depicted in Figure 7b. According to these spectra, there are regions with lower and higher fluorescent intensity, in agreement with the corresponding images: zone A presents a higher intensity than zone B, which is higher than zone C (supposed to be nonfluorescent). This weak fluorescence appears due to scattering from the illuminated vicinity. We also obtained the fluorescence spectra through the transversal section of the film surface: the upper focus being on one face of the film, the lower focusing on the other surface, and a third focusing on the bulk. This trend of the spectral intensity provides an evaluation of the phase composition across the film sample.[17] Figure 7c depicts these spectra for the three foci discriminated in Figure 7b. The inversion of the relative intensity observed for region A, compared to the region C, shows that an inverted concentration profile occurs from one surface to the other: the surface where region A is copolymer-richer and region C is copolymer-poorer, and vice versa. This also means that phase interconnection takes place in the entire sample.

The morphology of the EMAS/PS blend containing 20 wt % of EMAS (shown in Figure 7d,e) is slightly different from blends with MMAS/PS with the same composition: interconnection between the domains is less evident by epifluorescence for the unannealed sample although the PS-richer phase (nonfluorescent) is clearly interconnected after annealing. Larger fluorescent domains with assorted diameters ranging from 20 to 100 $\mu$m were occluded within the interconnected phase.

In a previous work,[24] blends of nBMAS/PS with 20 wt % of copolymer showed a morphology with interconnected regions, and two miscible phases with distinct relative compositions are observed. In addition, it seems that there is an increase of morphologic uniformity as the size of the ester−aliphatic chain increases in this

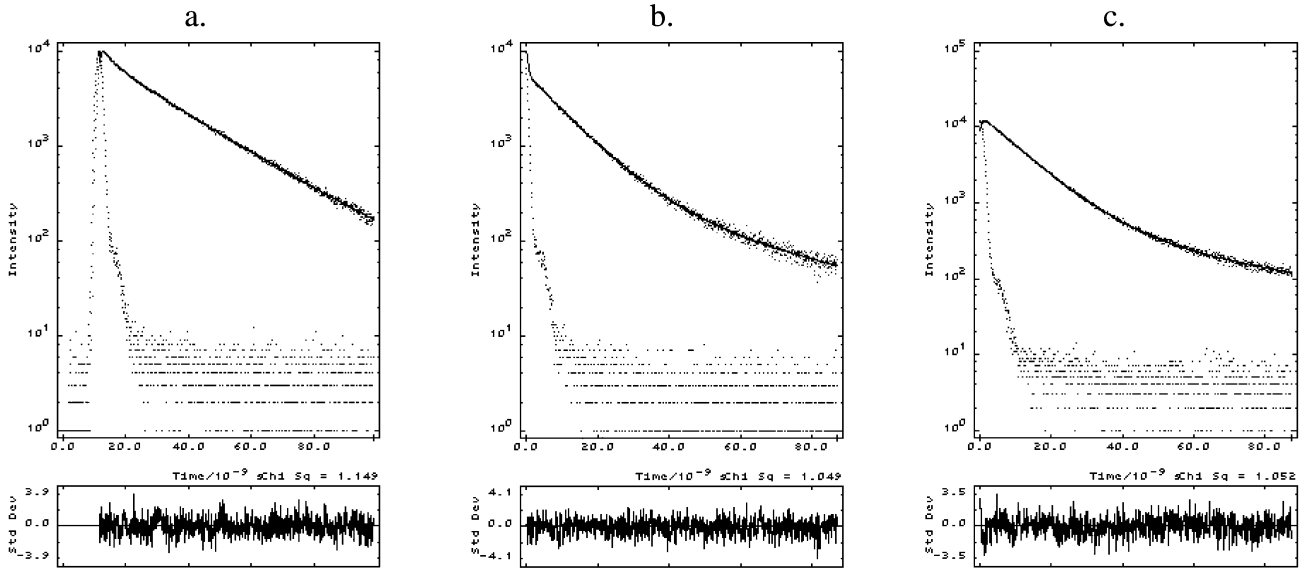


**Figure 5.** Fluorescence decays of (a) PS monitored at $\lambda_{em} = 340$ nm and of (b) MMAS and (c) EMAS monitored at $\lambda_{em} = 420$ nm and $\lambda_{exc} = 262$ nm.

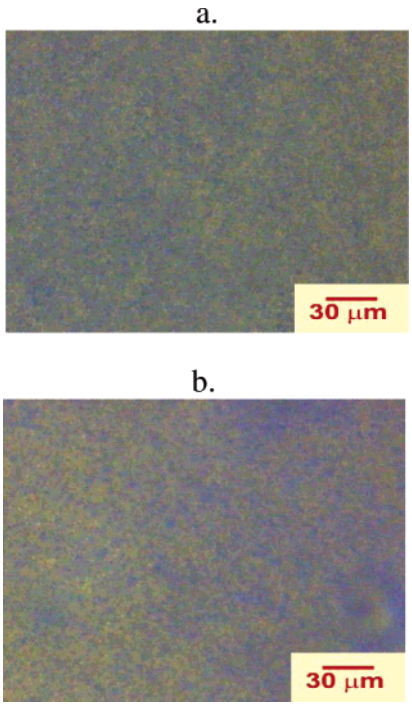


**Figure 6.** EFM micrographs of MMAS/PS (a) and EMAS/PS (b) blend with 5 wt % XMAS.

composition. Further evidence for this statement was obtained from dynamic fluorescence decays.

DSC traces for blends of 20% EMMAS/PS show a sharp glass transition (trace 5 in Figure 2b) with a single $T_g$ value between those of the neat polymers (Table 2). Differently, DMTA data (trace 5 in Figure 3b) provided two $T_g$ values, both between the $T_g$ of the neat components, strongly suggesting a morphology of two miscible phases with distinct relative compositions.

Microfluorescence spectra of this blend recorded in different parts of the sample and also at different depths from the surface support the results obtained from the $T_g$-based techniques. The fluorescence intensity decreases (Figure 7f) with the distance from one face to the other when spectra are collected focusing the microscope over a strongly fluorescent zone (B region

**Table 2. Glass Transition Temperatures ($T_g$) of PS, Copolymers, and MMAS/PS and EMAS/PS Blends Determined by DSC and DMTA**

| | MMAS/PS | | EMAS/PS | |
|---|---|---|---|---|
| composition | $T_g$ (DSC) (°C) | $T_g$ (DMTA) (°C) | $T_g$ (DSC) (°C) | $T_g$ (DMTA) (°C) |
| 0/100 | 91 (13)[a] | 95 | 91 (13) | 95 |
| 5/95 | 82 (12) | 65 | 72 (12) | 66 |
| | | 85 | | 85 |
| 20/80 | 87 (28) | 77 | 75 (11) | 59 |
| | | 85 | | 79 |
| 50/50 | 60 (8) | 59 | 61 (8) | 40 |
| | 85 (8) | 92 | 86 (8) | 60 |
| | | | | 73 |
| 80/20 | 83 (25) | 61 | 68 (13) | 73 |
| | | 93 | | |
| | | 109 | | |
| 95/5 | 92 (24) | 65 | 73 (24) | 70 |
| | | 104 | | |
| 100/0 | 85 (16) | 103 | 61 (17) | 73 |

[a] Values between parentheses are the width of the transitions (difference between final and initial transition temperatures) from DSC traces.

in Figure 7e) or over the interconnected regions (A and C zones in Figure 7e) (Figure 7f). From the thermal analysis and microspectroscopic data we can describe this blend as a biphasic system, composed by two miscible phases with distinct composition: one low-fluorescent matrix (PS-richer) containing dispersed copolymer-richer domains.

EFM images of annealed samples of 50 wt % MMAS/PS and EMAS/PS blends (Figure 8a,d) are very similar to larger size and broader size droplet distribution compared with blends with lower copolymer compositions. These large droplets are almost nonfluorescent (PS-richer material) dispersed in a more fluorescent matrix (Figure 8b,e) of copolymer-richer phase. Although with lower fluorescence intensity, magnification of the larger droplet images shows that they are also formed by smaller emissive dispersed droplets over a nonfluorescent matrix, reproducing the same behavior as the macroscopic domains. We explain the formation of this morphology by a two-step phase separation by nucleation and growth mechanism, forming

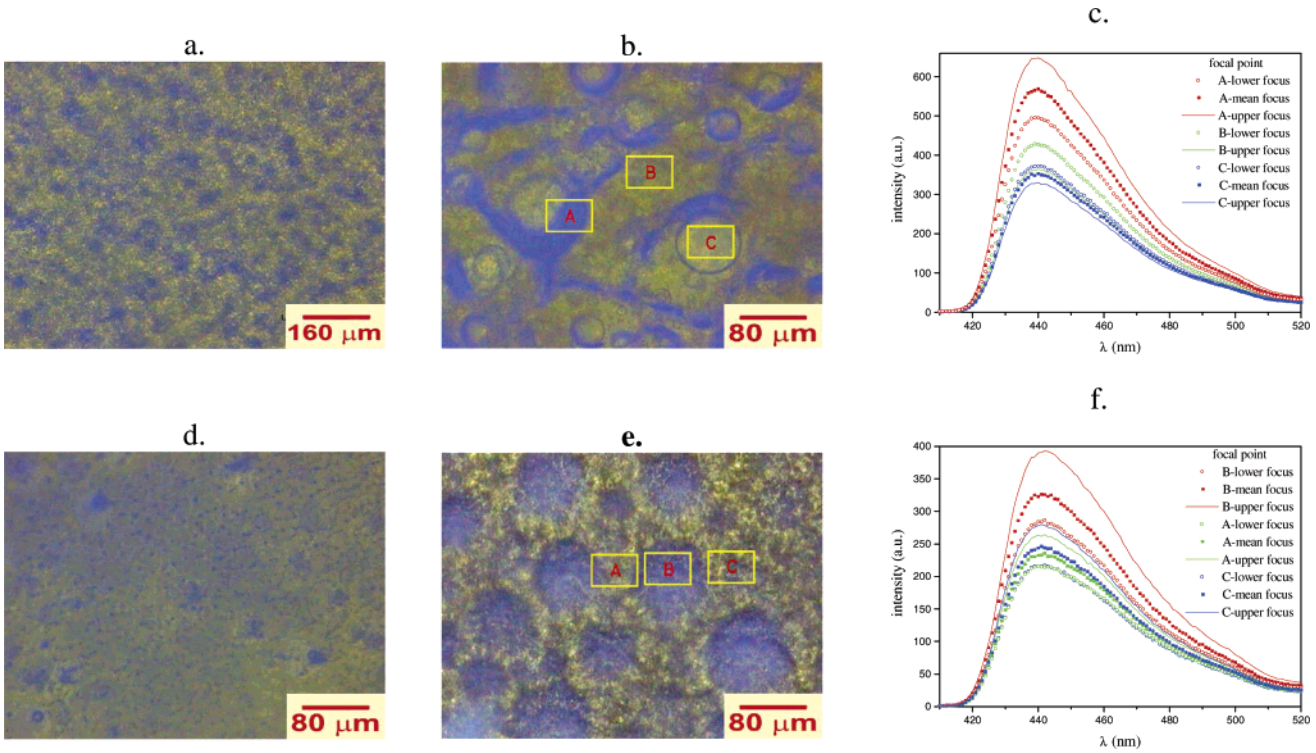


**Figure 7.** EFM micrographs of MMAS/PS and EMAS/PS blends with 20 wt % of copolymer: MMAS/PS blend (a) before and (b) after annealing; EMAS/PS blend (d) before and (e) after annealing. Fluorescence microspectra of the regions specified in micrographs b and e: (c) MMAS and (f) EMAS copolymers. Microspectroscopy was performed at three different depths: top (surface), bulk, and bottom (inferior surface).

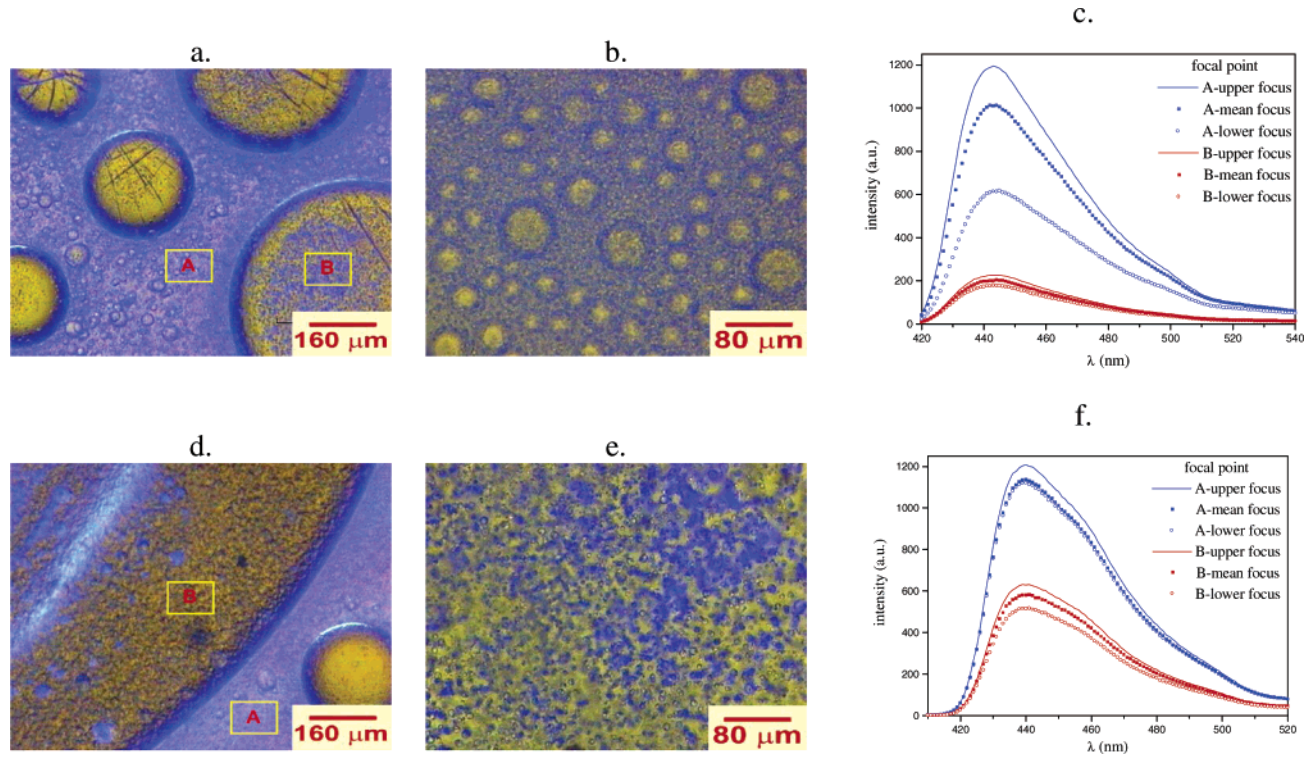


**Figure 8.** EFM micrographs of annealed blends with 50 wt % of copolymer: (a) MMAS/PS blend and (b) magnification of microzone A of (a); (d) EMAS/PS blend and (e) magnification of microzone B in (d). Microfluorescence spectra at three different depths: top (surface), bulk, and botton (inferior surface) of (c) MMAS (a) and (f) EMAS (d) copolymers.

large gelified droplets, which undergo a sequential secondary separation that, depending on the composition, produces droplets dispersed in a matrix (Figure 8b) or interconnected phases (Figure 8e). Furthermore, it is also remarkable that the interfaces between the phases present highly fluorescent rings in contact with the highly fluorescent matrix and an almost nonfluorescent ring in contact with the lesser-fluorescent droplets, which are often ascribed to the exclusion zones.[16]

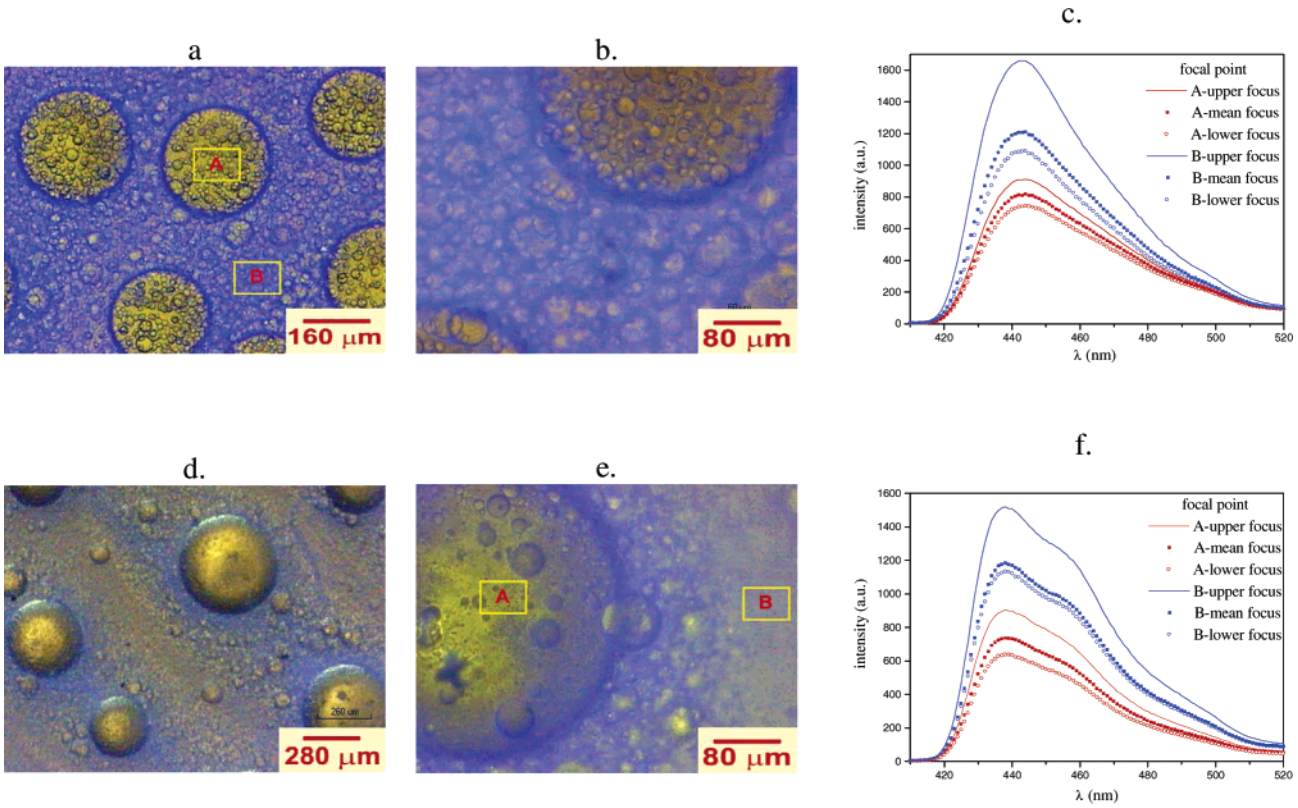


**Figure 9.** EFM micrographs of annealed blends with 80 wt % of copolymer: (a) MMAS/PS blend and (b) magnification of (a); (d) EMAS/PS blend and (e) magnification of (d). Microfluorescence spectra at three different depths: top (surface), bulk, and bottom (inferior surface) of (c). MMAS (a) and (f). EMAS (d) copolymers. Zones are defined in (b) and (e).

Two glass transitions arise from the DSC (trace 4 in Figure 2a,b) and DMTA (trace 4 in Figure 3a,b) traces for the XMAS/PS blends with 50 wt % of copolymer with two $T_g$ values between those from the neat components (Table 2), giving further evidence of a biphasic system. The higher $T_g$ value is assigned to the larger droplets of the PS-richer phase and the lower value to the fluorescent matrix (copolymer-richer phase).

Fluorescence microspectroscopy of the 50 wt % MMAS and EMMS blends were recorded in two positions defined in Figure 8a,d and shown in Figure 8c,f: in zone A (copolymer-richer phase, highly fluorescent) the fluorescence intensity decreases with the depth across the film; within the droplets (zone B), the fluorescence emission is lower and the fluorescence intensity is almost independent of the focus depth. According to the DMTA data and to the EFM micrographs, we conclude thath this is a triphasic system formed by a fluorescent matrix (copolymer-richer phase), nonfluorescent droplets (PS phase), and lower fluorescent smaller droplets inside the larger droplets (PS-richer phase).

A similar morphology of large droplets over a highly fluorescent matrix was obtained in previous work with the nBMAS/PS blend of symmetric composition.[23] However, different from the present work, the annealing process performed a significant rule on the final morphology of the nBMAS/PS blend, since the $T_g$ of both materials possessed values very apart one from other, leading to a more immiscible blend system than that before the annealing. Even so, taking into account the results from DSC measurements, nBMAS/PS blends are supposed to be more miscible than MMAS/PS and EMAS/PS having a symmetrical composition.

Similar morphologies with a fluorescent matrix containing less-fluorescent droplets are also observed with images from EFM for blends with 80 wt % of MMAS/PS and EMAS/PS, even after annealing (Figure 9). Despite their similarity, there are larger sizes and wider size distributions of the droplets in EMAS/PS blends. Sizes of these droplets present diameters up to 430 $\mu$m (Figure 9d,e) while for the MMAS blend two size distributions are seen, from 130 to 280 $\mu$m (Figure 9a) and from 30 to 80 $\mu$m (Figure 9b). Again, secondary phase separation is observed inside the droplets (Figure 9b,e). The sharp differences arise due the exclusion zones existing over a large portion in the EMAS/PS blend, where small, slightly fluorescent droplets are distributed around the larger domains, as is shown in Figure 9b. The other important difference that arises from the images is the exclusion zone around the droplets, which are more diffuse for the EMAS blend, suggesting larger interphase diffusion between PS and copolymer.

In comparison with the previous study of nBMAS/PS blends with 80 wt % nBMAS, the morphologies of the MMAS/PS and EMAS/PS blends are virtually insensitive to the annealing process, as also seen with the symmetrical composition. However, it is clear that the effect of the annealing process is more pronounced for this composition than for the symmetrical one. Therefore, prior to the annealing process, the nBMAS/PS blend with 80 wt % copolymer is supposed to be more miscible than other XMAS/PS blends, although further experimental evidence is necessary to give more consistency to this prediction.

The DSC trace for the MMAS/PS blend (trace 3 in Figure 2a) exhibits a broad glass transition with a $T_g$ value near the neat MMAS copolymer (Table 2). Nevertheless, the DMA data for this blend (trace 3 in Figure 3a) resulted in three $T_g$ values (Table 2), showing that,

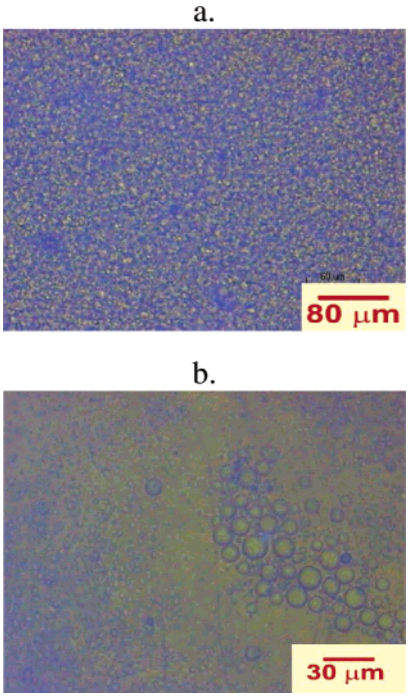


**Figure 10.** EFM micrographs of annealed blends with 95 wt % of copolymer: (a) MMAS/PS and (b) EMAS/PS blends.

besides the presence of the segregated components, miscibility over the entire matrix is possible. The DSC trace for the EMAS/PS blend (trace 3 in Figure 2b) shows one $T_g$ value at 68 °C, in agreement with the DMA data (trace 3 in Figure 3b).

Figure 9c,f exhibits the spectra obtained by fluorescence microspectroscopy for the MMAS/PS and EMAS/PS blends with 80 wt % of copolymer of two selected zones: within the droplets and at the matrix. As with the 50 wt % blend, in the zone B, composed of a copolymer richer-phase, highly fluorescent, the fluorescence intensity decreases with depth across the film; within the droplets (zone A), the fluorescence emission is lower, and the fluorescence intensity also decreases with the focus depth.

Epifluorescence micrographs for the annealed MMAS/PS and EMAS/PS blends with 95 wt % of copolymer (Figure 10c,d) follow the trend: droplets (smaller due to the lower concentration of PS) of lower luminescent material dispersed in a more highly fluorescent matrix (copolymer-richer phase). The MMAS/PS blend exhibits a more uniform morphology (although heterogeneous) of fluorescent and nonfluorescent phases. Again, further magnification of the less fluorescent phase reveals small spherical domains consisting of weakly fluorescent material, indicating a secondary phase separation process.

The DSC traces for the blends with 95 wt % of copolymer (trace 2 in Figure 2a,b) show a single glass transition (Table 2) that is broader relative to $T_g$ values for the neat components. On the contrary, except for the EMAS-rich, the DMTA data (trace 2 in Figure 3a) exhibit two glass transitions (Table 2), in agreement with the epifluorescence images.

Combining the results from thermal analysis and from epifluorescence microscopy, we conclude that XMAS/PS blend with 95 wt % copolymer is also a biphasic system. Different from the others compositions, the tendency to higher miscibility for the XMAS/PS blends with 95 wt % copolymer seems to follow the reverse rule; i.e., the nBMAS/PS blend of a previous work, whose nBMAS copolymer possesses a longer aliphatic ester chain, has shown three $T_g$ values from DSC trace and a morphology with secondary phase separation and, thus, is supposed to be more immiscible than other XMAS/PS blends that contain smaller aliphatic ester chains.

**Micromorphology and Energy Transfer Processes.** In the previous topic, we discussed the miscibily of the XMAS/PS blends in terms of thermal analysis and epifluorescence images. Thermal analysis was based on the determination of the glass transition temperatures and the technique measures dispersion states on a micrometric scale. Besides being of low sensitivity, other experimental difficulties concerned with broad transitions and the overlap of $T_g$ in immiscible blends may arise. Furthermore, if one component is present in a very small quantity, it may not be detected.[34] Because of these intrinsic difficulties, correlation between microscopy and thermal analysis cannot be straightforward.

In an attempt to overcome this difficulty, we consider the possibility of energy transfer processes between the excimer phenyl groups of the PS phase and the anthryl moieties of the copolymers. As previously shown, the copolymer intrachain energy transfer is not considered since there is no excimer emission (see Figure 4), and emission from the electronically excited phenyl groups is improbable due to the lower spectral overlap with the excitation band of the anthryl.

The nonradiative energy transfer processes (NRET) is strongly dependent on the spatial arrangement of the D−A pairs (donor−acceptor) and only occurs over a spatial range of a few nanometers.[12] Therefore, interpenetrations between phases (that require miscibility) take place at the molecular level, and consequently, NRET is indicative of local miscibility. One type of NRET occurs through the Förster mechanism (dipole−dipole interaction) with an efficiency $\epsilon$ that increases with the decrease of the distance $R$ between excimer phenyl groups (donor) and 9-anthryl moieties (acceptor):

$$\epsilon = \frac{R_0^6}{R_0^6 + R^6} \tag{4}$$

where $R_0$ is a parameter (Förster distance) that is characteristic of each donor−acceptor pair, given by

$$R_0^6 = \frac{9.000 k^2 Q_D \ln 10}{128 \pi^5 n^4 N_A} \int \frac{F_D(\tilde{\nu})\, \epsilon_A(\tilde{\nu})}{\tilde{\nu}^4}\, d\tilde{\nu} \tag{5}$$

where $\tilde{\nu}$ is the wavenumber, $\epsilon_A(\tilde{\nu})$ is the molar absortivity coefficient of the acceptor absorption, $F_D(\tilde{\nu})$ is the normalized fluorescence band of the donor, $\Phi_D$ is the fluorescence quantum yield of the donor in the absence of acceptor, $N_A$ is Avogrado's number, $n$ is the refractive index, and $k^2$ is an orientation factor whose value is $^2/_3$ for random directional distribution. For the polystyrene (donor) and 9-methylanthracene (acceptor) pair, the Förster distance $R_0 = 1.54$ nm.[35] According eqs 4 and 5, the energy transfer efficiency depends on the spectral overlap integral between the emission from the donor and the absorption of acceptor: $J = \int F_D(\tilde{\nu})\, \epsilon_A(\tilde{\nu})/\tilde{\nu}^4\, d\tilde{\nu}$, which represents the spectral overlap between the excimer emission and the absorption of anthryl moieties (see dark region in Figure 4). It is well established that

**Table 3. Fluorescence Lifetimes for the Excimer in MMAS/PS and EMAS/PS Blends Collected at 340 nm (Excimer Phenyl Groups) (Using $\lambda_{exc}$ = 262 nm) Obtained by Distribution Analysis**

| | | composition | | | | |
|---|---|---|---|---|---|---|
| | | 5/95 | 20/80 | 50/50 | 80/20 | 95/5 |
| MMAS/PS | $\langle\tau_i\rangle$ (ns) | 2.8 ± 0.2 (4.3%)[a] | 2.8 ± 1.1 (4.9%) | 2.7 ± 0.2 (6.1%) | 4.3 ± 0.1 (9.0%) | 4.5 ± 1.1(12.4%) |
| | | 11.0 ± 1.6 (32.2%) | 16.2 ± 5.8 (95.1%) | 14.4 ± 1.9 (59.0%) | 16.5 ± 0.9 (60.7%) | 23.5 ± 9.6 (69.6%) |
| | | 20.3 ± 2.9 (63.5%) | | | | |
| | $\chi^2$ | 1.08 | 1.13 | 1.13 | 1.09 | 1.11 |
| EMAS/PS | $\langle\tau_i\rangle$ (ns) | 3.2 ± 0.1 (3.1%) | 3.6 ± 0.1 (3.4%) | 3.4 ± 0.1 (5.0%) | 4.6 ± 0.1 (5.6%) | |
| | | 11.8 ± 0.8 (36.7%) | 11.6 ± 1.5 (42.4%) | 13.9 ± 1.1 (48.8%) | 14.5 ± 1.5 (43.0%) | |
| | | 21.9 ± 1.5 (60.2%) | 22.7 ± 2.5 (54.2%) | | | 20.7 ± 15.3 (96.7%) |
| | $\chi^2$ | 1.25 | 1.14 | 1.02 | 1.14 | 1.12 |

[a] The percentages in parentheses refer to the relative contributions of each component.

a high quantum efficiency for the NRET process leads to a considerable decreasing of fluorescence intensity of the donor when in the presence of an acceptor. However, measurements of NRET by steady-state spectroscopy are difficult in the present case because the selective excitation of the donor cannot be completely performed due to some spectral overlap with the higher energy states of the acceptor.[36]

Nevertheless, the energy transfer efficiency can also be evaluated from the fluorescence lifetime measurements:

$$\epsilon = 1 - \frac{\tau_{DA}}{\tau_D} \tag{6}$$

where $\tau_D$ is the fluorescence lifetime of the donor (excimer phenyl groups) in the absence of acceptor (9-anthryl moieties) and $\tau_{DA}$ is the fluorescence lifetime of the donor in the presence of acceptor.

The use of eq 6 predicts that the decays of the donor will be here a single exponential in both the absence ($\tau_D$) and in the presence ($\tau_{DA}$) of acceptor only if there is a single value for the distance between the donor−acceptor pairs. Consequently, the existence of several possible distances among the donors and acceptors must result in more complex decays, which can be described either by multiexponential functions or by a continuous distribution of lifetimes. Because the decays observed in this work cannot be fitted by single or even by double exponentials, we decided to use distribution analysis to fit the experimental data, and the average value $\langle\tau_i\rangle$ of the excimer lifetime in the absence (PS homopolymer) ($\langle\tau_{PS}\rangle$ = 21.0 ± 4.7 ns) will be compared with the value in the presence of acceptors (copolymer). If a decrease of lifetime is observed in polymer blends, interpenetration of PS and copolymer phases has occurred as well as some degree of miscibility.

As already shown, the fluorescence lifetime of the excimer emission in PS in the absence of the acceptors was determined from the fit of the curves in Figure 5. In Table 3, we show the lifetimes of the excimer emissions that resulted from the distribution analysis of blends with several compositions. In several cases at least two mean lifetime components arise from the data treatment: one of these components is shorter (from 2.7 to 4.5 ns) and can be assigned to the singlet−singlet annihilation process also observed for the PS homopolymer.[28] The second component is intermediate between the singlet−singlet annihilation and the normal excimer emission. This shorter decay, compared with the normal excimer emission, is associated with the decay of the donor (excimer) in the presence of the acceptor (anthryl moieties) located within the Förster distance. Furthermore, whereas the shorter components (up to 4.5 ns) are supposed to be independent of the blend and composition, the longer lifetimes depend on the blend and composition.

Figure 11a shows the fluorescence lifetime distribution for excimer phenyl groups of the XMAS/PS blends with 5 wt % of copolymer, which is a partially miscible material, as already anticipated by DSC and DMTA data and epifluorescence images (Figure 6). Distribution analysis of lifetimes (Table 3) shows two narrow average components (excluding the annihilation component): 11.0 ± 1.6, 20.3 ± 2.9 ns (MMAS/PS) and 11.8 ± 0.8, 21.9 ± 1.5 ns (EMAS/PS). The shorter lifetime component is attributed to the excimer emission strongly quenched by the 9-anthryl groups by the NRET process in the miscible interconnected fluorescence while the longer matches PS homopolymer $\langle\tau_{PS}\rangle$ (21.0 ± 4.7 ns) and is attributed to the lifetime of excimers located in the immiscible phase. Besides the information about chain interpenetration, two significant features from these lifetime distribution are noteworthy: (i) since they are narrow, it implies narrow D−A distance distributions in the mixed phase and, consequently, a large amount of styryl units and 9-anthryl moieties separated by the Förster distance (1.54 nm); (ii) the narrow PS-like component show that this blend contains at least one miscible phase, which is in agreement with the DMTA and EFM images.

The fluorescence lifetime distributions for the excimer phenyl groups from the XMAS/PS blends with 20 wt % of copolymer are depicted in Figure 11b. Broader monomodal and bimodal lifetime distributions are obtained for the MMAS/PS and EMAS/PS, respectively. For MMAS an average fast decay of 16.2 ± 5.8 ns, compared to neat PS, is observed, in addition to the singlet−singlet annihilation (2.8 ± 1.1 ns). Again, excluding the S−S annihilation, the faster decay is associated with the miscible phase of the blend, in agreement with the thermal analysis and with the epifluorescence images (Figure 7a,b). On the other hand, the bimodal distribution of the longer decay observed for 20 wt % EMAS/PS blend gives two average components: 11.6 ± 1.5 ns associated with the miscible phase and 22.7 ± 2.5 ns similar to and associated with the PS homopolymer immiscible phase. This observation is compatible with the epifluorescence images (Figure 7d,e) that show interconnected lower fluorescence domains, characteristic of the PS-richer phase. It also suggests the absence of sharper interfaces in the MMAS/PS blend, and as a consequence of the broader distribution of lifetimes, we also expect a wide distribution of distance among the donor and acceptor groups, in agreement with the cocontinuous morphology.

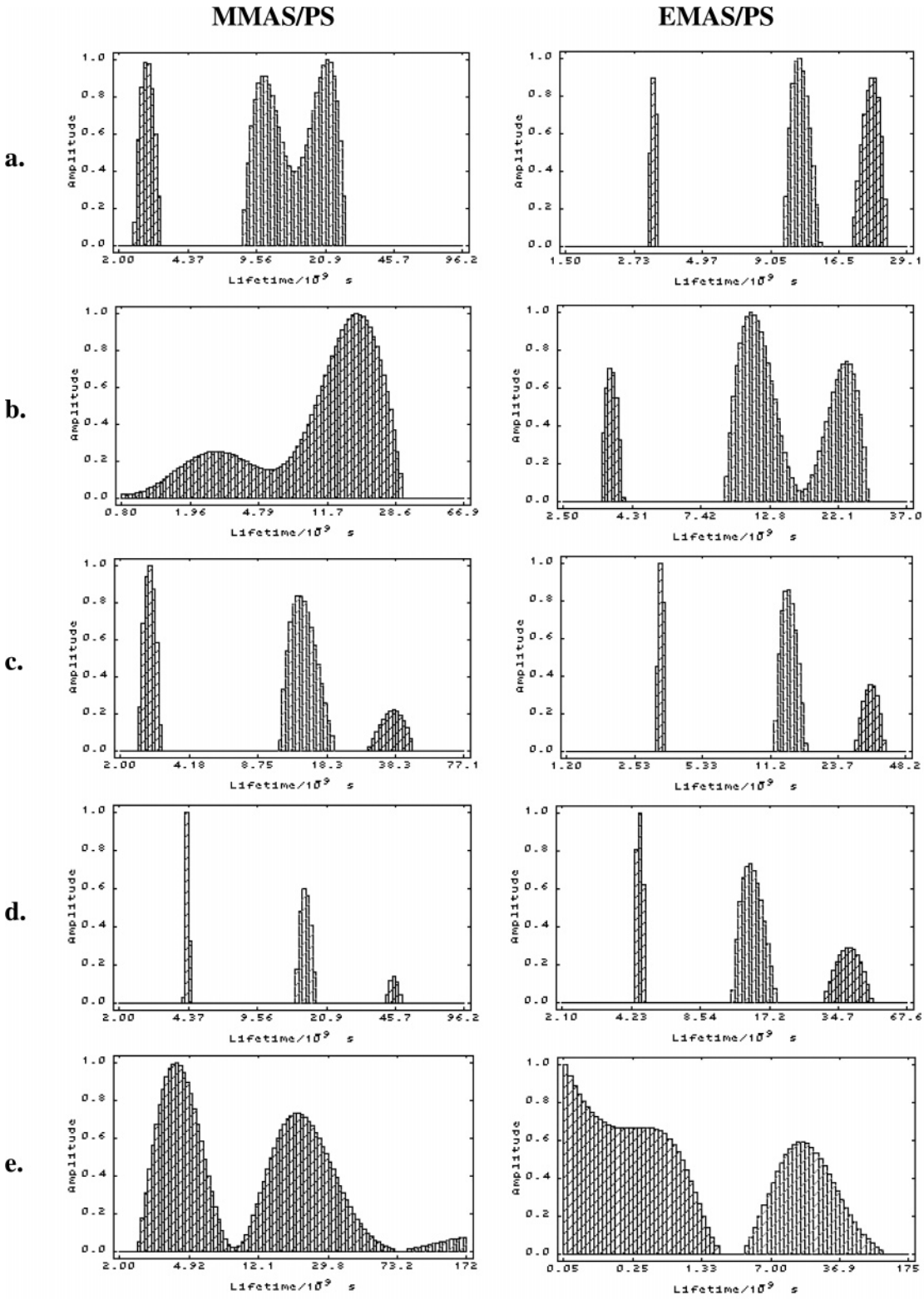


**Figure 11.** Fluorescence lifetime distribution for the excimer phenyl emissions ($\lambda_{exc}$ = 262 nm, $\lambda_{em}$ = 340 nm) of the XMAS/PS blends: (a) 5/95, (b) 20/80, (c) 50/50, (d) 80/20, and (e) 95/5.

XMAS/PS blends with 50 and 80 wt % of copolymers show fluorescence lifetime for the excimer emission with bimodal narrow distributions of the decays: one attributed to S−S annihilation and a longer one, of approximately 14−16 ns (Figure 11c,d), also associated with the energy transfer between excimer and anthryl groups in the miscible phase or at the interface between the droplets and the matrix, as shown by the epifluorescence microscopy images.

MMAS/PS and EMAS/PS blends containing 95 wt % XMAS, with thermal properties and morphology show zones with miscibility and also zones totally immiscible, exhibit broader lifetime distributions whose average value is characteristic of the excimer emission: $\langle\tau_{PS}\rangle$ = 23.5 ± 9.6 ns and $\langle\tau_{PS}\rangle$ = 20.7 ± 15.3 ns for MMAS and EMAS, respectively (Figure 11e,f). Again, a broader lifetime distribution reflects the heterogeneity of the donor/acceptor distance, some of them within the ex-

pected value of the Förster radius, leading to faster lifetimes and other far from this distance, decaying with the natural excimer lifetime. Faster lifetime results of the NRET require interchain interpenetration and miscibility in agreement with the morphologies shown in Figure 10.

In the previous work with nBMAS/PS blends[23] very broad lifetime distributions of excimer fluorescence for both PS-rich blends (5 and 20 wt %) were observed. Different from the XMAS/PS blends in this work (which possess shorter ester group aliphatic chain on the copolymer), the former did not show a bimodal aspect. Besides this, a broadening of the fluorescence lifetime distributions for 9-anthryl groups in these compositions was also observed, which suggested several types of microenvironments around the 9-anthryl groups. Therefore, it becomes clearer that the miscibility of the blend, and hence the specific interaction, increases as the ester group aliphatic chain of the copolymer increases in PS-richer compositions, following an increasing order of polarity of the medium. Nevertheless, this rule is not the same in copolymer-rich compositions, where the XMAS/PS blends are considered immiscibles at both the micrometric level and the nanometric level. With regard to the symmetric composition, the nBMAS/PS blend was shown to be more miscible than its XMAS/PS analogous blends before the annealing process, as shown by broad fluorescence lifetime distributions.

**Remarks on Copolymer Structural Effect.** The overall interaction parameter $B$ for a blend comprised of the homopolymer PS and the copolymer XMAS is given by the pseudobinary interaction model:[37]

$$B = B_{\mathrm{XMA-S_1}}\phi'_{\mathrm{XMA}} + B_{\mathrm{S_2-S_1}}\phi'_{\mathrm{S}} - B_{\mathrm{XMA-S_2}}\phi'_{\mathrm{XMA}}\phi'_{\mathrm{S}} \quad (7)$$

where the $\phi'_i$ describe the copolymer composition; $\phi'_{\mathrm{XMA}} + \phi'_{\mathrm{S}} = 1$, and the subscripts 1 and 2 denote the styrene monomer coming from PS homopolymer and XMAS copolymer, respectively. According to this model, in the limit of high molecular weight, PS and XMAS are miscible only if mixing is exothermic, i.e., $B < 0$, which requires that either a mutual repulsion occurs between the constituents (copolymer units) of the copolymer (very high and positive value of $B_{\mathrm{XMA-S_2}}$) or specific interactions occur between the components leading to an exothermic heat of mixing (negative or relatively small values of $B_{\mathrm{XMAS-S_1}}$ and $B_{\mathrm{S_2-S_1}}$).

Here we assume that the miscibility of PS with XMAS occurs due the combination of the two effects abovementioned, being the former (specific interaction) already elucidated. Because the interaction energies between PS and acrylates follow the order PnPMA < PEMA < PnBMA < PMMA, and hence, the miscibility should increase as PnPMA > PEMA > PnBMA > PMMA.[5]

The copolymer effect (mutual repulsion) can be explained in terms of dipole−dipole interaction between the copolymer segments and homopolymer when the two chains/segments are very close. Because the chain segment of the XMAS copolymer consist of some number of the two different attached mers (styrene and alkyl methacrylate), the polarity of the XMAS copolymer is a statistical average between the two monomers in a random combination.[38] A favorable intermolecular interaction may be expected if the polarity in the XMAS copolymer is close to or matches that of the PS homopolymer. Semiempirical calculation showed that dipole moment of nBMA−S segments is lower than of EMA−S and MMA−S segments, and hence the polarity of such nBMAS copolymer segments in a random combination is more likely that of the PS homopolymer increasing this miscibility.

Furthermore, Braun and co-workers[39] showed (by using binary interaction model) that the shorter styrene segments affecting the interactions in binary blends with XMAS copolymers is the styrene−styrene dyads. Because the use of free radical reaction in the synthesis of all copolymers, the S−XMA sequences follows a random distribution with blocks of each monomer predominantly syndiotact, which is confirmed by $^{13}C$ NMR spectra. In addition, since we do not observe excimer emission of the styrene blocks of the copolymer, we conclude that these are an alternate random copolymer with short blocks of styrene mers. Blocks of alternating structure must become more likely by the enhancing of steric hindrance between the aliphatic ester groups and phenyl rings. Therefore, in nBMAS copolymer, such steric hindrance leads to a copolymer with chains containing a larger amount of S−XMAS syndiotact sequences, and hence a larger amount of $\pi$-electron cloud of phenyl rings is not screened by the ester groups. As a result, the surface of specific interactions between the styryl segments on the different macromolecules is larger for the copolymer of larger aliphatic ester group. These assumptions are in agreement with our spectroscopic observations and morphological analysis showing that the miscibility with PS follow the order nBMAS > EMAS > MMAS.

## Conclusions

The morphology and the miscibility of the blends of XMAS [X = M (methyl), E (ethyl)] with PS were studied in several compositions (5−95 wt % PS) on the micrometric scale using epifluorescence microscopy (EFM), differential scanning calorimetry (DSC), dynamic-mechanical thermal analysis (DMTA), and dynamic fluorescence spectroscopy. By combining epifluorescence microscopy and steady-state fluorescence spectroscopy, we have clearly shown that two miscible interconnected phases with distinct composition is observed for XMAS/PS blends (5 and 20 wt % XMAS), whereas at least two miscible phases (droplets dispersed in a matrix) is observed for blends with 50 and 80 wt % XMAS. For blends with symmetric composition there is a secondary phase separation inside the PS-richer droplets. By using fluorescence lifetime distribution analysis based on the Förster mechanism, we observed that fine structures exist only in the XMAS/PS blends with 5 wt % XMAS on the submicroscopic length scale and seems to be cocontinuous. The results from this work (MMAS/PS and EMAS/PS blends), together with the previous work (nBMAS/PS blends), indicate that the miscibility increases as the ester group aliphatic chain of the copolymers increases for PS-rich XMAS/PS blends, following a increasing order of polarity of the medium.

**Acknowledgment.** T.D.Z.A. and M.L.A. thanks FAPESP, CNPq, MCT/PADCT/IMMP, and FAEP/UNICAMP for financial support and fellowships. We also thank Prof. Carol Collins for useful discussions.

## References and Notes

(1) Takeaki, A.; Hajime, T. *Macromolecules* **2001**, *34*, 1953.

(2) Utracki, L. A. In *Polymer Alloys and Blends: Thermodynamics and Rheology*; Hanser: Munich, 1989; Chapter 2.
(3) (a) Benabdelghani, Z.; Belkhiri, R.; Djadoun, S. *Polym. Bull. (Berlin)* **1995**, *35*, 329. (b) Robertson, C. G.; Wilkes, G. L. *Polymer* **2000**, *41*, 9191. (c) Ziaee, S.; Paul, D. R. *J. Polym. Sci., Part B: Polym. Phys.* **1996**, *34*, 2641. (d) Li, G. X.; Cowie, J. M. G.; Arrighi, V. *J. Appl. Polym. Sci.* **1999**, *74*, 639.
(4) (a) Fukuda, T.; Inagaki, H. *Pure Appl. Chem.* **1983**, *55*, 1541. (b) Fukuda, T.; Nagata, M.; Inagaki, H. *Macromolecules* **1984**, *17*, 548. (c) Fukuda, T.; Nagata, M.; Inagaki, H. *Macromolecules* **1986**, *19*, 1411.
(5) Kim, J. H.; Park, D. S.; Kim C. K. *J. Polym. Sci., Part B: Polym. Phys.* **2000**, *38*, 2666.
(6) Serrano, B.; Baselga, J.; Pierola, I. F. *Polym. J.* **2002**, *34*, 905.
(7) (a) Vukovic, R.; Bogdanic, G.; Karasz, F. E.; Macknight, W. J. *J. Phys. Chem. Ref. Data* **1999**, *28*, 851. (b) Tenbrinke, G.; Karasz, F. E.; Macknight, W. J. *Macromolecules* **1983**, *16*, 1827. (c) Kim, C. K.; Kim, J. J.; Paul, D. R. *Polym. Eng. Sci.* **1994**, *34*, 1788.
(8) Nishimoto, M.; Keskkula, H.; Paul, D. R. *Polymer* **1991**, *32*, 1274.
(9) (a) Alam, M. M.; Tonzola, C. J.; Jenekhe, S. A. *Macromolecules* **2003**, *36*, 6577. (b) Ding, L.; Karasz, F. E.; Lin, Z.; Liao, M. Z. L.; Pang, Y. *Macromolecules* **2001**, *34*, 9183. (b) Yu, J.-W.; Kim, J. K.; Cho, H. N.; Kim, D. Y.; Kim, C. Y.; Song, N. W.; Kim, D. *Macromolecules* **2000**, *33*, 5443. (c) Aihara, S.; Kamata, N.; Nishibori, A.; Nagumo, K.; Sato, H.; Terunuma, D.; Yamada, K. *J. Lumin.* **2000**, *87*−*9*, 745. (d) Anni, M.; Gigli, G.; Paladini, V.; Cingolani, R.; Barbarella, G.; Favaretto, L.; Sotgiu, G.; Zambianchi, M. *Appl. Phys. Lett.* **2000**, *77*, 2458. (e) Aoki, H.; Ito, S. *J. Phys. Chem. B* **2001**, *105*, 4558. (f) Cleave, V.; Yahioglu, G.; Le Barny, P.; Hwang, D. H.; Holmes, A. B.; Friend, R. H.; Tessler, N. *Adv. Mater.* **2001**, *13*, 44.
(10) Aoki, H.; Kunai, Y.; Ito, S.; Yamada, H.; Matsushige, K. *Appl. Surf. Sci.* **2002**, *188*, 534.
(11) Tcherkasskaya, O.; Ni, S.; Winnik, M. A. *Macromolecules* **1997**, *30*, 2623.
(12) Webber, S. E. *Chem. Rev.* **1990**, *90*, 1469.
(13) (a) Farinha, J. P. S.; Vorobyova, O.; Winnik, M. A. *Macromolecules* **2000**, *33*, 5863. (b) Feng, J. R.; Winnik, M. A.; Siemiarczuk, A. *J. Polym. Sci., Part B: Polym. Phys.* **1998**, *36*, 1115. (c) Atvars, T. D. Z.; Esteban, I.; Illera, B.; Serrano, B.; Vigil, M. R.; Piérola, I. F. *J. Lumin.* **1997**, *72*−*4*, 467.
(14) (a) Pekcan, O. *Eur. Polym. J.* **1996**, *32*, 117. (b) Pekcan, O. *Chem. Phys.* **1993**, *177*, 619. (c) Pekcan, O. *J. Appl. Polym. Sci.* **1993**, *49*, 151.
(15) Kulkarni, A. P.; Jenekhe, S. A. *Macromolecules* **2003**, *36*, 5285.
(16) Cassagnau, P.; Michel, A. *Polymer* **2001**, *42*, 3139.
(17) Fukui, Y.; Murata, M. *Appl. Catal., A* **2002**, *237*, 1.
(18) Pawley, J. *J. Microsc.* **1984**, *136*, 45.
(19) Hemsley, D. A. In *The Light Microscopy of Synthetic Polymers*; Oxford University Press: Oxford, UK, 1984; Chapter 2.
(20) (a) Dibbern-Brunelli, D.; Atvars, T. D. Z. *J. Appl. Polym. Sci.* **1995**, *58*, 779. (b) Dibbern-Brunelli, D.; Atvars, T. D. Z.; Joekes, I.; Barbosa, V. C. *J. Appl. Polym. Sci.* **1998**, *64*, 645.
(21) Cruz, M. C. P.; Cassiola, F. M.; Atvars, T. D. Z. *J. Appl. Polym. Sci.* **2002**, *84*, 1637.
(22) Granados, E. G.; González-Benito, J.; Baselga, J.; Dibbern-Brunelli, D.; Atvars, T. D. Z.; Esteban, I.; Piérola, I. F. *J. Appl. Polym. Sci.* **2001**, 949.
(23) de Andrade, M. L.; Atvars, T. D. Z. *J. Phys. Chem. B*, in press.
(24) Reddy, G. V. R.; Joseph, V. S.; Mani, K. C. *J. Appl. Polym. Sci.* **2000**, *77*, 398.
(25) *Polymer Handbook*; Brandrup, I. J., Immergut, E. H. II; McDowell, W., Eds.;Wiley-Interscience Publication, John Wiley & Sons Inc.: New York, 1975.
(26) Sircar, A. K.; Drake, M. L. *ACS Symp. Ser.* **1990**, *424*, 132.
(27) (a) Christoff, M.; Atvars, T. D. Z. *Macromolecules* **1999**, *32*, 6093. (b) Itagaki, H. *Macromolecules* **1991**, *24*, 6531.
(28) (a) Zhang, G.; Thomas, J. K. *J. Phys. Chem.* **1995**, *99*, 11203. (b) Birks, J. B. In *Photophysics of Aromatic Molecules;* Wiley-Interscience: New York, 1970. (c) Semerak, S. N.; Frank, C. W. *Adv. Polym. Sci.* **1984**, *54*, 31. (d) Hirayama, F. *J. Chem. Phys.* **1965**, *42*, 3726.
(29) de Deus, J. F.; Andrade, M. L.; Atvars, T. D. Z.; Akcelrud, L. *Chem. Phys.* **2004**, *297*, 177.
(30) (a) Yuan, H.; Párkányi, L. C.; Guo, R. K.; Wu, F. P. *J. Photochem. Photobiol. A: Chem* **1992**, *63*, 45. (b) Kamat, P. V. *Anal. Chem.* **1987**, *59*, 1636.
(31) Aspler, J. S.; Hoyle, C. E.; Guillet, J. E. *Macromolecules* **1978**, *11*, 925.
(32) Kwei, T. K.; Wang, T. I. In *Polymer Blends*; Paul, D. R., Newman, S., Eds.; Academic Press: Orlando, FL, 1979; Vol. I, pp 141−183.
(33) (a) Jang, F. H.; Woo, E. M. *Polymer* **1999**, *40*, 2231. (b) Woo, E. M.; Su, C. C. *Polymer* **1996**, *37*, 4118.
(34) Chartoff, R. P. In *Thermal Characterization of Polymeric Materials*, 2nd ed.; Turi, E. A., Ed.; Academic Press: San Diego, CA, 1997; p 542.
(35) Berlman, I. B. In *Energy Transfer Parameters of Aromatic Compounds*; Academic Press: New York, 1973.
(36) Platt, J. R. *J. Chem. Phys.* **1949**, *17*, 484.
(37) (a) Paul, D. R., Newman, S., Eds. In *Polymer Blends*; Academic: New York, 1978; Vol. 1. (b) Sanchez, I. C.; Lacombe, R. H. *Macromolecules* **1978**, *11*, 1145.
(38) (a) Callaghan, T. A.; Paul, D. R. *Macromolecules* **1993**, *26*, 2450. (b) Callaghan, T. A.; Paul, D. R. *J. Polym. Sci., Part B: Polym. Phys.* **1994**, *32*, 1813.
(39) Braun, D.; Yu, D.; Kohl, P. R.; Gao, X.; Andradi, L. N.; Manger, E.; Hellmann, G. P. *J. Polym. Sci., Part B: Polym. Phys.* **1992**, *30*, 577.

MA049265E